ACS APPLIED MATERIALS & INTERFACES

Research Article

www.acsami.org

Small Temperature Coefficient of Resistivity of Graphene/Graphene Oxide Hybrid Membranes

Pengzhan Sun,[†] Miao Zhu,[†,‡] Kunlin Wang,[†] Minlin Zhong,[†] Jinquan Wei,[†] Dehai Wu,[†] and Hongwei Zhu*[,†,‡]

[†]School of Materials Science and Engineering, Key Laboratory for Advanced Manufacturing by Materials Processing Technology, and [‡]Center for Nano and Micro Mechanics, Tsinghua University, Beijing 100084, China

Supporting Information

ABSTRACT: Materials with low temperature coefficient of resistivity (TCR) are of great importance in some areas, for example, highly accurate electronic measurement instruments and microelectronic integrated circuits. In this work, we demonstrated the ultrathin graphene−graphene oxide (GO) hybrid films prepared by layer-by-layer assembly with very small TCR (30−100 °C) in the air. Electrical response of the hybrid films to temperature variation was investigated along with the progressive reduction of GO sheets. The mechanism of electrical response to temperature variation of the hybrid film was discussed, which revealed that the interaction between graphene and GO and the chemical doping effect were responsible for the tunable control of its electrical response to temperature variation. The unique properties of graphene−GO hybrid film made it a promising candidate in many areas, such as high-end film electronic device and sensor applications.

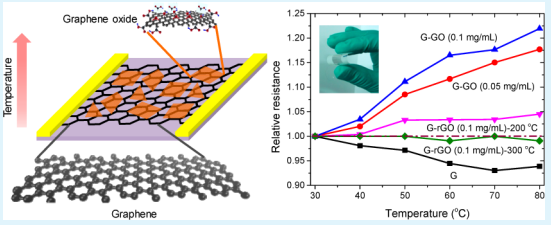

KEYWORDS: *graphene, graphene oxide, hybrid, temperature coefficient of resistivity*

1. INTRODUCTION

Currently, thermal issue has become one of the most important problems in the electronic industry for high-end electronic devices due to their advancement of designs within the nanometer scale. And the self-heating of nanosized electronic devices is one of the most challenging obstacles to further increase the performance of integrated circuits because increasing temperature could diminish the performance of the electronic device significantly. In order to solve these problems, materials have been developed and advanced rapidly to have a low temperature coefficient of resistivity (TCR), which is crucially important in some areas, for example, highly accurate electronic measurement instruments and microelectronic integrated circuits,[1−3] for the reason that electrical robustness against temperature variation is required in these areas. However, the currently existing low TCR materials mainly are metal alloys[4] and metal oxide ceramic,[5] which possess many intrinsic problems, such as the oxidation on metal surface and poor adhesion because of the structural strain. Low TCR properties are all characterized under vacuum by a commercial quantum design physical property measurement system, which restricts their practical applications in the air. However, the thickness of most current thin film resistors on these low TCR materials is above 100 nm, which is not real two-dimensional (2D) and further restricts their applications in flexible, transparent 2D electronic devices. It is well-known that if the thickness of a certain material is reduced to nanoscale, a large percentage of atoms will be exposed to surface and the adsorbed molecules will change the local carrier concentration, which will result in the significant change in resistance. In addition, a thinner film exhibits poor continuity which degrades the performance significantly. Therefore, it is of great significance to develop some new ultrathin 2D materials (<10 nm) with low TCR.

Graphene[6] has stimulated extensive research interests since the first isolation of the individual graphene plane in 2004 due to its unique structure and excellent properties, which make it a promising candidate for the next generation of electronic devices. Because of the successful synthesis of large-area graphene films with high quality via chemical vapor deposition (CVD),[7,8] it is possible to fabricate large-area and macroscopic electronic devices. Moreover, the protection of graphene films from air oxidation will significantly enlarge the range of its practical applications.[9] Graphene oxide (GO),[10−12] prepared through chemical routes, has been demonstrated to be another type of promising 2D nanomaterial due to its excellent properties, such as easiness to synthesize and scale up. Especially, GO can be manipulated in liquid phase and reassembled into monolayer through methods such as layer by layer (LBL) electrostatic self-assembly.[13,14] Notably, properties of GO can be tuned precisely through reduction to various degrees, to realize the transition from insulator to semimetal.[15−17] These properties of GO flakes ensure its versatile potential applications in electronic devices.

When graphene film and GO [or reduced GO (rGO)] are hybridized together through LBL method, the unique structure

Received: June 23, 2013
Accepted: September 9, 2013
Published: September 9, 2013

   dx.doi.org/10.1021/am403186r | ACS Appl. Mater. Interfaces 2013, 5, 9563−9571

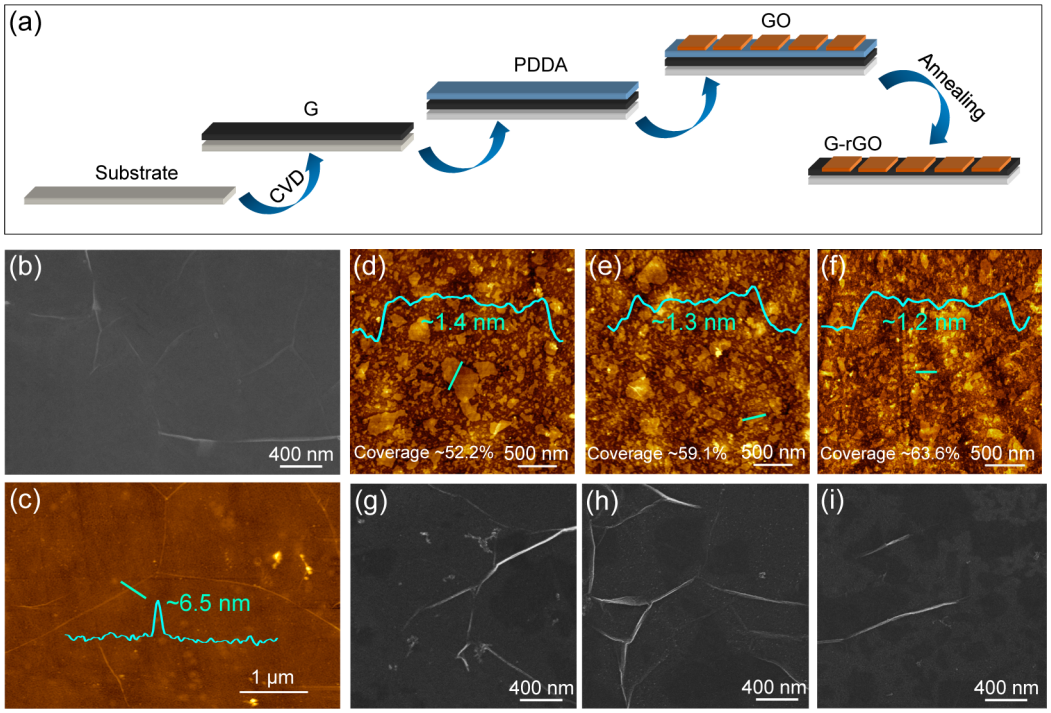

Figure 1. (a) Schematic of the preparation of graphene–GO hybrid films by LBL method. (b) SEM and (c) AFM characterizations of the as-prepared graphene films. The inset in (c) shows the corresponding height profile of the surface wrinkles. (d–f) GO sheets deposited on Si wafers via LBL method using GO colloidal suspensions with a concentration of 0.05, 0.1, and 0.2 mg/mL, respectively. (g–i) Graphene–GO hybrid films prepared by LBL method using GO solutions with a concentration of 0.05, 0.1, and 0.2 mg/mL, respectively.

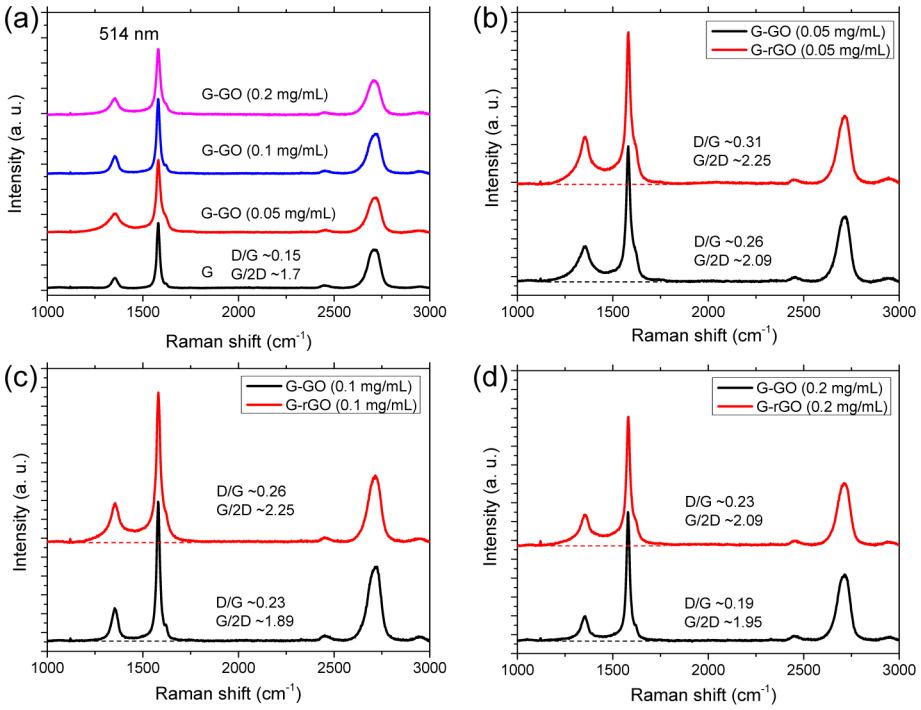

Figure 2. (a) Raman spectra of graphene and graphene–GO hybrid films with different GO coverage densities on graphene films (excited by 514 nm laser line). Graphene–GO hybrid films prepared by LBL method using GO suspensions with a concentration of (b) 0.05 mg/mL, (c) 0.1 mg/mL, and (d) 0.2 mg/mL before and after thermal reduction at 300 °C for 30 min.

of monolayer GO sheets deposited on graphene matrix is realized. The possible interactions between these two 2D nanomaterials and the notable adsorption/desorption effects in the air might lead to the generation of some novel electrical properties. In addition, the controllable alterability of the electronic properties of the hybrid films may be realized based on the reduction of GO flakes to various degrees.

In this work, ultrathin graphene–GO (–rGO) hybrid films prepared by using LBL method with very small TCR (30–100 °C) in the air have been demonstrated. Electrical response of

dx.doi.org/10.1021/am403186r | ACS Appl. Mater. Interfaces 2013, 5, 9563–9571

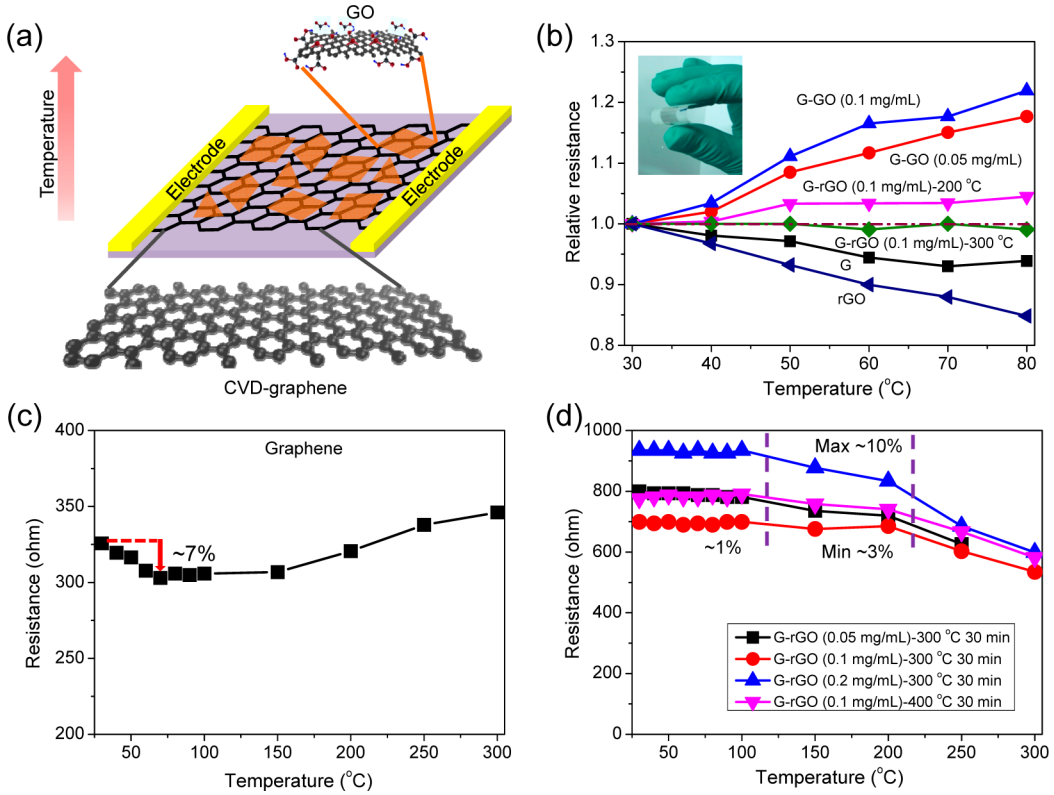

Figure 3. (a) Schematic diagram for the electronic properties test during the heating process. (b) Relative resistances of graphene–GO (–rGO) hybrid films in the range of 30–80 °C obtained by nomalizing with the resistances at 30 °C. (c) Resistances of bare graphene films in the range of 30–300 °C. (d) Resistances of graphene–rGO hybrid films in the range of 30–300 °C.

the hybrid films to temperature variation was investigated with the progressive reduction of GO flakes to different extents. Mechanism of the electrical response of hybrid films to temperature was systematically discussed. The properties of graphene–GO (–rGO) hybrid film made it a promising candidate in some areas, such as high-end film electronic devices and sensor applications. To the best of our knowledge, this would be the first systematical study to demonstrate graphene–rGO hybrid films as ultrathin low TCR materials.

2. RESULTS AND DISCUSSION

2.1. Microscopic Characterizations of Graphene–GO Hybrids. Graphene film was prepared by CVD method under an atmospheric pressure.[18] The free-standing graphene film was transferred onto quartz wafer for the subsequent GO deposition. Monolayer GO flake was prepared by a modified Hummers' method using the wormlike graphite as carbon source.[19,20] Due to ionization of the oxygen-containing functional groups on GO, the as-prepared GO flake was negatively charged in its aqueous suspension, which facilitated its LBL electrostatic self-assembly process with graphene film to produce ultrathin graphene–GO hybrid film.

The detailed LBL process to fabricate graphene–GO hybrid film is shown in Figure 1a (see Experimental Section). SEM and AFM images of the as-prepared graphene film are shown in Figure 1b and c. As shown in these two panels, the surface was smooth with some surface wrinkles. The height of the surface wrinkle was ~6.5 nm according to the inset in Figure 1c. Figure 1d–f shows AFM images of the as-prepared GO sheets deposited on Si wafers by LBL method in which GO solutions with different concentrations (0.05–0.2 mg/mL) were used as the GO source. It revealed that most of the as-prepared GO sheets had thickness of ~1 nm, which demonstrated the monolayer nature. As the concentration of the GO source was increased, the coverage density of the substrate was increased. Similar results can also be found in Figure S1a–c in the Supporting Information. Based on these results, we could fabricate graphene–GO hybrid films with different GO coverage densities by controlling the concentration of GO solution in the LBL process, which could be utilized to tune properties of the hybrid films, as shown in Figure 1g–i. The results showed that GO sheet was adhered uniformly on the graphene surface and the increased concentration of GO suspension in the LBL process led to the increase of coverage density on graphene surface, which indicated that the structural property of graphene–GO hybrid film could be tuned through the LBL method. Particularly, during the LBL process, the GO sheet could be deposited uniformly on the wrinkles of graphene film, which could be utilized to alter the electronic transport in polycrystalline graphene. Further detailed information (SEM/TEM images and UV–vis absorption/transmission spectra) of graphene–GO hybrid film is provided in Figures S1 and S2.

The typical Raman spectra of graphene–GO hybrid film are shown in Figure 2. After the hybridization with GO sheet, D peaks became broadened compared to that of bare graphene film and then gradually overlapped with G peaks, which indicated the successful hybridization of graphene and GO sheets. Additionally, the intensity ratios of D/G and G/2D were increased, indicating the increase of defect density and layer number of the hybrid films compared to that of graphene films. After the annealing at 300 °C for 30 min, GO sheets on graphene films were reduced to rGO and PDDA interlayers

dx.doi.org/10.1021/am403186r | ACS Appl. Mater. Interfaces 2013, 5, 9563–9571

between graphene and GO sheets were removed completely at the same time. As shown in Figure 2b–d, the D peaks were further overlapped with G peaks and the intensity ratios of D/G and G/2D were increased, which suggested that more defects (i.e., vacancies and small holes) were generated during the thermal reduction process. Due to the complete removal of PDDA layers, graphene and rGO sheets could be adhered tightly to form polymer-free graphene–rGO hybrid films.

According to the above characterizations, we concluded that ultrathin graphene–GO hybrid film could be fabricated via the LBL method and GO sheets could be deposited uniformly on the surface of graphene film. Increasing the concentration of GO source during the LBL process could result in the increase of GO coverage density on graphene surface, which led to the generation of hybrid film with tunable structure. Notably, GO sheets could be deposited uniformly on the wrinkles of graphene film, which might have potential applications in manipulating electronic transport in polycrystalline graphene. As GO sheets could be thought as graphene that was decorated with oxygen-containing functional groups, these functional groups could be gradually removed and sp^2 conjugated graphene network would be partially restored during the thermal reduction process, which would result in the transition from insulator to semimetal in graphene oxide. And this transition would change the manners of charge transportation and generate tunable electronic properties within the hybrid films.

2.2. Temperature Dependent Resistance Measurement. The electrical responses to temperature variation of graphene–GO (–rGO) hybrid films with different GO coverage densities and various extents of thermal reduction were investigated, as shown in Figure 3a (see Experimental Section). Temperature dependent current–voltage (I–V) results of the hybrid film are displayed in Figure 3b–d. The resistance responses to temperature (30–80 °C) of graphene–GO (–rGO) hybrid films were shown in Figure 3b. For graphene films, the temperature increase would result in the decrease of resistance and the maximum resistance variation was ~7%. However, after the hybridization with GO sheets, the temperature increase led to the monotonic increase of resistance, which was just in contradiction to that of graphene. In addition, when GO coverage density was increased, the resistance change became larger and the maximum variation was increased from ~18% to ~22%, which was much larger than that of graphene film. The significant enhancement of electrical response to temperature endows graphene–GO hybrid film with potential applications in thermal sensors. During the progressive thermal reduction of graphene–GO hybrid films (200 °C for 30 min, then 300 °C for another 30 min), the resistance variations under different temperatures were decreased. Surprisingly, after the reduction of graphene–GO hybrid film at 300 °C for 30 min, its resistance could be kept almost constant from 30 to 80 °C (actually from 30 to 100 °C in Figure 3d), which demonstrated the excellent electrical stability of graphene–rGO hybrid film under thermal disturbance. The TCR values of graphene–rGO hybrid films obtained from the equation of $\rho_0^{-1}(d\rho/dT)$, where ρ_0 is the resistivity at 30 °C, are shown in Table 1. Comparing with the previous reported low TCR materials, the TCR value of graphene–rGO (0.1 mg/mL) hybrid film annealing at 300 °C (0.23 ppm/K) is 1–3 orders of magnitude smaller than those of metal alloys and metal oxide ceramic and is comparable to the optimum case of RuO_x (0.12 ppm/K).[1−5] Detailed I–V characterizations of these studied samples under different temperatures are shown in Figures S3 and S4, which revealed the tunable electrical response to temperature variation. Because the thermal stability (low TCR nature) is crucially important for high-end electronic devices and sharp fluctuation of electronic property with temperature declines the performance of electronic devices significantly, graphene–rGO hybrid film is a promising candidate in accurate electronic device fabrication due to its excellent thermal stability.

Table 1. TCR values of Graphene–rGO Hybrid Films Compared with the Previous Reported Low TCR Materials

samples	TCR (ppm/K)
G-0.05rGO-300 °C	−325
G-0.1rGO-300 °C	0.23[a]
G-0.2rGO-300 °C	−77
G-0.1rGO-400 °C	99.8
$CuNMn_3$	46
$Ga_{0.95}CFe_3$	−5.72
$Ga_{0.85}Al_{0.15}CFe_3$	−14.68
$GaCFe_3$	46.2
RuO_2–TiO_2	−557.17 to −54.92
NiCr	~10
RuO_x	0.12[a]

[a]The TCR value of graphene–rGO (0.1 mg/mL) hybrid film annealing at 300 °C (0.23 ppm/K) is comparable to the optimum case of RuO_x (0.12 ppm/K). Please see the text.

To further investigate the thermal stability of graphene–rGO hybrid film, the resistance responses of graphene (Figure 3c) and graphene–rGO hybrid film with different GO coverage densities (Figure 3d) were examined within a larger range of temperature variation (30–300 °C). As shown in Figure 3c, when temperature was increased, the resistance of graphene film was decreased at first (to an extent of ~7%) and then increased subsequently (to an extent of ~15%), which revealed the relative large fluctuation of electronic property and the inconstant change tendency with temperature variation of graphene film. However, in the case of graphene–rGO hybrid film (Figure 3d), as temperature was increased, resistances of all the tested samples were almost kept constant at the beginning (30–100 °C) and the maximum resistance variation was less than 1%. Then, from 100 to 200 °C, the resistance was decreased gradually, but the variation was relatively small (3–10%). Finally, from 200 to 300 °C, the resistance was further decreased subsequently. An enlarged version of Figure 3d is shown in Figure S5, which reveals the details of resistance change of graphene–rGO hybrid film. It is worth noting that the electrical responses of graphene–rGO hybrid films were conducted under the same temperature per day, which demonstrated the relative electrical stability of graphene–rGO hybrid films against temperature variations. Moreover, the resistance tendency and the maximum resistance variation were unchanged when the thermal reduction temperature was increased from 300 to 400 °C, which suggested that 300 °C was enough for the fabrication of hybrid film with outstanding thermal stability. These results indicated that the resistance of graphene film varied sharply with temperature and the change tendency was not constant, while the resistance of graphene–rGO hybrid film was constant in the range of 30–100 °C and then decreased subsequently, which further demonstrated the excellent thermal stability of graphene–rGO hybrid film. And the hybrid film possessed other extraordinary properties, such

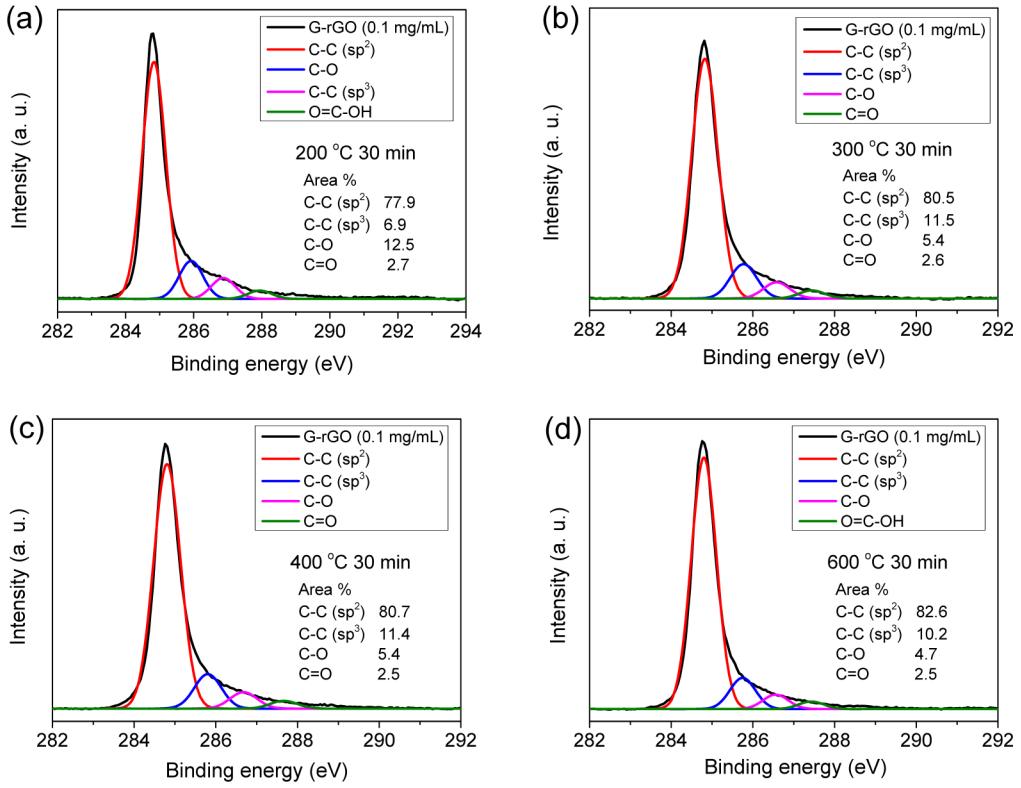

Figure 4. XPS spectra of graphene–rGO hybrid films after thermal reduction at (a) 200 °C, (b) 300 °C, (c) 400 °C, and (d) 600 °C for 30 min.

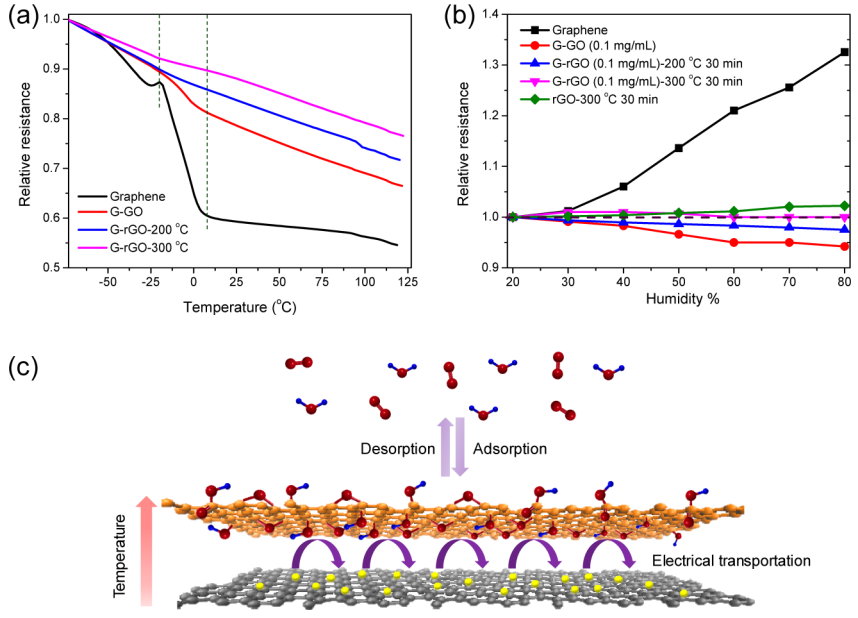

Figure 5. (a) Relative resistance–temperature curves of graphene–GO (–rGO) hybrid films in vacuum. (b) Relative resistance–humidity curves of graphene and graphene–GO (–rGO) hybrid films. (c) Model for the electronic modulation of the graphene–GO (–rGO) hybrid film.

as ultrathin thickness, good flexibility, high transmittance and excellent conductivity. Especially, the hybrid film was effective protected to avoid its oxidation with air. All of these excellent properties of graphene–rGO hybrid film could significantly enlarge its potential applications in electronic industry.

2.3. Mechanism of Small TCR. The mechanism of electrical response of graphene–GO (–rGO) hybrid film to temperature variation was studied as well. First, the chemical structures of graphene and its hybrid film with GO (rGO) sheet were investigated via XPS spectra, as shown in Figures 4 and S6. In the case of graphene–GO hybrid film that was prepared by LBL method using 0.1 mg/mL GO suspension as the source (Figure 4), increasing the reduction temperature from 200 to 600 °C resulted in the decrease of oxygen-containing functional groups. These results indicated that the oxygen functional groups on GO (rGO) sheet and the interaction between graphene and GO might play very important roles in the modulation of electronic properties of graphene–GO (–rGO)

dx.doi.org/10.1021/am403186r | ACS Appl. Mater. Interfaces 2013, 5, 9563–9571

hybrid film. More detailed information about the XPS spectra of graphene film, GO sheet, and graphene−rGO film with different GO coverage densities is shown in Figure S6.

In order to further investigate the mechanism of resistance change of the hybrid film at various temperatures, the resistance−temperature curves were obtained under vacuum by using a commercial quantum design physical property measurement system as shown in Figure 5a. This result revealed that, as the temperature was increased from −70 to 120 °C, resistance of all the samples exhibited a decreasing tendency under vacuum. In detail, as the temperature was increased, the resistance of graphene film was decreased and then dropped off steeply in the range of −20−7 °C; beyond 7 °C, the resistance was decreased relatively slowly. However, after the hybridization with GO sheet, the resistance slumping became much gentler. In addition, as the thermal reduction temperature increases from 200 to 300 °C, the resistance variation in the range of −20 to 7 °C gradually became gentler, which indicated that the hybridization with GO and rGO sheets could strongly alter the electron transportation in polycrystalline graphene films. However, as the resistance of graphene−GO (−rGO) hybrid film followed different manners with increasing temperatures in air and under vacuum, the molecular adsorption and desorption effect should be responsible for the modulation of electronic properties of hybrid film.

Finally, based on graphene and its hybrid film with GO and rGO sheets, a molecular adsorption experiment was conducted with water vapor, which further demonstrated the above hypothesis. The sample was moisturized by using a humidifier and the humidity around the samples was captured simultaneously. The $I-V$ curve was measured, and the resistance under certain humidity was calculated, which is plotted in Figure 5b. For graphene films, the resistance increased monotonously with humidity, and rGO film (prepared by drop-casting followed by thermal reduction) also increased with the same manner. While the resistance of graphene−GO hybrid film responded in an adverse form and the resistance variation became much smaller. After the hybrid film was partially reduced (200 °C), increasing the humidity resulted in the decrease of resistance and the maximum variation was decreased further compared to that of the oxidized form. When the hybrid film was reduced at 300 °C, the resistance again remained constant in the humidity range of 20−80%. The above results were just opposite to the resistance change with temperature increasing as shown in Figure 3b, which demonstrated that molecular desorption during the heating process played an important role in the modulation of electronic properties of graphene−GO (−rGO) hybrid films.

Basing on the results of previous experiments, we proposed a theoretical model for the modulation of electronic properties of graphene−GO (−rGO) hybrid films (Figure 5c). The as-prepared graphene film via CVD had a polycrystalline nature in which the formed grain boundary network (mainly pentagon-hexagon pairs and dislocations) divided the graphene film into highly conductive single-crystalline grains. And these highly conductive single-crystalline grains were isolated by many resistive interface regions with several nanometers in width.[21] Crossing the grain boundaries, the Brillouin zone of the charge carrier experienced a significant rotation and the conductivities for both electrons and holes at the grain boundaries were significantly suppressed due to the short-range and intervalley scattering of the charge carrier in the defective grain boundary regions.[22−24] All of these caused a significant impediment of electrical transport in polycrystalline graphene film, which led to a remarkable decrease in conductivity compared to that single-crystalline grain. While, the GO sheet structure of monolayer GO flakes could be thought as intact, highly conductive graphene islands of several nanometers were separated by an amorphous and highly defective sp^3 bonded matrix.[15−17,25] During the thermal reduction, oxygen-containing functional groups were gradually removed and the sp^2 conjugated graphene network was partially restored, which resulted in an increased number of localized states and the absence of delocalization of carriers.[16] Therefore, charge transfer in reduced GO sheets might occur via a variable-range hopping mechanism which involved the consecutive inelastic tunneling processes of charge carriers between two localized states.[15−17,25] As the reduction process advanced, an increased number of hopping sites would be generated which facilitated the occurrence of hopping process. When graphene and GO sheets were hybridized together via LBL method, a layer of PDDA molecules was intercalated between them and an AFM topography characterization of PDDA molecules on graphene surface was shown in Figure S7. According to the XRD spectra of GO_{10} (10 layers of GO sheets were assembled together via the same LBL method as shown in Figure S8), after the annealing at 300 °C for 30 min, the diffraction peak shifted from 4.92° to 8.58°, corresponding to an interlayer thickness of ∼0.7 nm, which allowed the generation of charge carrier hopping process between graphene and GO sheet (Figure 5c).

Due to the thermal generation of electron−hole pairs, as shown in Figure 5a, the resistance of all the samples decreased under vacuum as the temperature was increased, which revealed their intrinsic semiconductor nature.[26,27] Furthermore, according to the previous results, the values and shapes of the resistance−temperature curves mainly depended on carrier scattering, disorders, and acoustic phonons.[26] When the temperature was decreased to ∼7 °C, the resistance of graphene film exhibited a steep enhancement (Figure 5a). This steep resistance increment was attributed to the kinetic energy decrease of these thermally excited carriers to the extent that most of these carriers were not able to span across the existing grain boundaries. Dramatically, when the graphene film was hybridized with GO sheets, because these as-deposited GO sheets could cover grain boundaries and wrinkles uniformly (Figures 1 and S1), charge carriers underneath the graphene film could effectively cross over the grain boundaries with the assistance of GO sheet via variable-range hopping process through the highly conductive, nanometer-sized graphene islands as shown in Figure 5c. Therefore, as the temperature was decreased, resistance of graphene-GO hybrid film increased much more gently around −20−7 °C compared to that of graphene film (Figure 5a). In addition, the thermal reduction resulted in conductivity enhancement of rGO sheets and the removal of PDDA layers, which facilitated the hopping process of charge carrier between graphene and rGO layer, thus led to the gradual gentler change and the relative increase of resistance around −20 to 7 °C (Figure 5a).

When graphene−GO (−rGO) hybrid films were heated in air (Figure 3b), the adsorbed molecules would change the local carrier concentration significantly and cause the chemical doping. And the adsorbed water layers on the surface of the hybrid film provided sufficient dielectric screening to suppress charge scattering on impurities, which led to the unaffected mobility with the increase of chemical doping.[28,29] In addition,

theoretical results had demonstrated that both H_2O adsorbate and the substrate were responsible for the chemical doping of hybrid film.[30,31] Based on these characteristics of chemical doping by molecular adsorption, the tunable electrical properties of the hybrid film could be explained as follows: In the case of graphene films (Figure 3b and c), the adsorbed water layer supplied solvated O_2 to graphene for the following redox reaction:[31,32]

$$O_2(aq) + 4H^+ + 4e^-(\text{graphene}) \leftrightarrow 2H_2O \quad (1)$$

According to the results mentioned above, the Fermi level of the electrons related to the above reaction (−5.3 eV) was lower than that of graphene (−4.6 eV), which led to the shift of graphene Fermi level into its valence band and then caused p-doping. Electrons would be transported from graphene to unoccupied levels of the solution until equilibrium was reached. During this reaction, highly reactive intermediate species (i.e., superoxide anions, peroxide, hydroxyl radicals) were generated, which tended to fix a negative charge on the substrate and stabilized a positive charge (hole) in graphene[31] (as illustrated in Figure S9). During the heating, H_2O adsorbates were gradually removed from the graphene surface and more electrons within graphene films were captured by O_2 molecules to promote more holes into the conduction band of graphene, which led to the resistance decrease of graphene film. However, as the heating process progresses, the molecular desorption of H_2O led to the removal of more O_2 molecules from graphene surface. Thus, the electronic density of O_2 was decreased and the solution Fermi level went up, resulting in the transfer of electrons from the occupied levels in the solution to the unoccupied levels of graphene, which caused the depletion of holes from the conduction band and increased the resistance of graphene film afterward (Figure 3b and c).

In the case of graphene−GO hybrid film (Figure 3b), the existing PDDA interlayers fixed a net positive charge on the graphene film and stabilized a negative charge in the GO sheet, which led to the effective n-doping of GO topmost layers. During the heating, H_2O molecules adsorbed on the surface were gradually desorbed and more electrons were withdrawn by O_2 molecules, leading to the resistance increase of graphene−GO hybrid film, which was just opposite to that of graphene film as shown in Figure 3b. In addition, as GO sheets were expected to contain a much larger amount of defects than graphene film and these defects serve as binding sites, interaction of small molecular adsorbate with GO sheet should be stronger than that with graphene film, which resulted in a larger sensitivity of graphene−GO hybrid film compared to graphene film (Figure 3b).

When graphene−GO hybrid film was extensively reduced above 300 °C, carbon losses during the thermal reduction process resulted in the widespread of point defects (i.e., vacancies, holes, etc.) throughout the whole film.[33] These point defects were expected to serve as strong binding sites for the adsorption of H_2O. Therefore, during the heating, O_2 was preferentially desorbed from surface solution on the hybrid film compared to H_2O due to the strong capture of the widely distributed point defects.[33] This process resulted in electron transportation from occupied states of the solution to unoccupied levels of the hybrid film. Because of the p-doping nature of the as-prepared graphene−rGO hybrid film in the air, the transferred electrons gradually neutralized the existing holes within the hybrid film, thus enhancing the resistance. On the other hand, the resistance of the hybrid film decreased with temperature increase under vacuum due to its semiconducting nature. The integrated result of these opposite effects resulted in the constant resistance of graphene−rGO hybrid film in the range of 30−100 °C, which was in agreement with our experimental results shown in Figure 3b and d. However, when the temperature was increased further, H_2O started to desorb from the surface of hybrid film, resulting in electron transfer from the occupied levels of hybrid film to the unoccupied states of solution. This reaction led to the gradual release of holes in hybrid films and this hole release caused the resistance decrease, which was in agreement with the results in Figure 3d.

Our interpretation could also be applied to the inverse process, the electrical response in the presence of water vapor, correctly. As shown in Figure 5c, for graphene film and rGO film, increasing the humidity resulted in the transportation of electrons from occupied levels of the surface solution to unoccupied states of graphene (rGO) layer (inverse reaction of eq 1). Due to the p-doping nature of the as-prepared graphene (rGO) film, the transferred electrons neutralized the holes within graphene (rGO) film gradually, leading to the enhancement of resistance. In the case of graphene−GO hybrid film, the positive charged PDDA interlayer stabilized a net negative charge in GO topmost layer, resulting in n-doping of the hybrid film. When the humidity was increased, the electron transfer from surface solution to hybrid film led to the reduction of resistance. Notably, due to the presence of C═O groups on GO and partially reduced rGO sheets that could trap electrons within the hybrid film effectively,[34] the maximum resistance variation of hybrid film was smaller than that of graphene film. After GO sheet in graphene-rGO hybrid film was reduced extensively above 300 °C, the widely distributed point defects provided strong binding sites for the effective capture of H_2O before moistening treatment. Therefore, due to the insufficient binding sites available on the rGO surface, few extra H_2O molecules were able to adsorb onto the hybrid films. Screening effect of the originally existing H_2O layer to the adsorption of extra water molecules resulted in a constant electrical property of graphene−rGO hybrid film with varied humidity.

Overall, we have fabricated graphene−GO (rGO) hybrid films via LBL method. The graphene film possessed extraordinary properties such as flexibility, large-area, high transmittance and excellent conductivity, and the as-synthesized monolayer GO flake was easy to scale up and could be manipulated in aqueous suspension. The properties of GO sheet could be successfully tuned by continuous reduction to various degrees, thus to realize the transition of GO sheet from insulator to semimetal. In addition, LBL procedure facilitated the hybridization of graphene and GO sheets at room temperature and the as-prepared graphene−GO hybrid film preserved the excellent properties of both graphene and GO sheets such as ultrathin thickness, flexibility (the inset in Figure 3b), high transmittance (Figure S2), high conductivity with the same magnitude as graphene. Above all, the successive and controllable alterability of electrical properties of hybrid film was the most amazing aspect. For example, the as-prepared graphene−GO hybrid film possessed superior temperature sensitivity compared to graphene film. When GO sheet were extensively reduced, the hybrid film would possess excellent thermal stability (low TCR nature) in the range of 30−100 °C and its electrical properties were insensitive to humidity. These properties made graphene−GO (−rGO) hybrid film as a promising candidate in many areas, such as the fabrication of

accurate microelectronic devices with high performance and sensor applications.

However, some problems are still required to be solved before the real application of graphene−GO (−rGO) hybrid film. For example, hybrid film on various substrates, including PET and other organic film materials, should be fabricated; and their electrical response to temperature should be investigated to further demonstrate the integrated effects of chemical doping and the interaction between graphene and GO sheet. So far, graphene−GO hybrid film on PET substrate have been successfully fabricated (the inset in Figure 3b) and thermoelectrical properties are investigated now, which might realize potential applications of the hybrid film in the fabrication of flexible high-end electronic devices. Moreover, it is necessary to investigate the electrical properties of graphene−rGO hybrid film because rGO sheets with different chemical structures (i.e., CN species by hydrazine reduction and point defects by thermal reduction) are expected to produce with different reduction methods. Furthermore, electronic transportation properties of graphene−GO hybrid film are not very clear so far and only few have ever been reported. More detailed theoretical studies are needed.

3. CONCLUSIONS

We fabricated graphene−GO hybrid films via LBL method at room temperature. The as-prepared graphene−GO (−rGO) hybrid film possessed extraordinary properties, such as ultrathin thickness, high transmittance, excellent conductivity and tunable electrical properties. The as-prepared graphene−GO hybrid film also possessed superior sensitivity to temperature variation compared to graphene, which made the hybrid film a promising candidate in some areas (e.g., sensor applications). On the other hand, graphene−rGO hybrid film exhibited excellent thermal stabilities (low TCR nature in the range of 30−100 °C) and they were insensitive to humidity, which could be applied in many areas, such as highly accurate electronic measurement instruments, microelectronic integrated circuits. Finally, the mechanism of electrical response to temperature variation of the hybrid film was discussed, which demonstrated that the interaction between graphene and GO (rGO) layer and the chemical doping effect were responsible for the tunable control of its electrical response to temperature variation. These amazing properties endowed graphene−GO (−rGO) hybrid films with excellent potential application in many areas, such as high-end film electronic devices, sensors, and other related applications.

4. EXPERIMENTAL SECTION

Preparation of Graphene. Graphene film was prepared by an atmospheric pressure CVD using copper foil as catalytic substrate and methane as the carbon source. After the growth process, the copper foil underneath the as-prepared graphene film was etched away by a mixture of $FeCl_3$ and HCl, which was followed by rinsing in deionized (DI) water for 3 h to completely remove the residual ions on the graphene film.

LBL Process. Prior to the LBL process, the substrates (Si and quartz wafers) were cleaned thoroughly in a bath of 1/1 methanol/HCl and concentrated H_2SO_4 solutions for 30 min, respectively. After that, the quartz wafer with a piece of adhered graphene film was immersed in a PDDA solution (20 g/L, pH ∼ 9) for 20 min to introduce positive charges on graphene and then thoroughly washed with DI water. The PDDA-treated graphene was then immersed in GO colloidal suspension (0.05−0.2 mg/mL, pH ∼ 9) for another 20 min and subsequently washed with water thoroughly. Finally, the as-prepared graphene−GO hybrid film was dried under nitrogen flow.

Temperature Coefficient of Resistivity Measurement. Two electrodes of silver paste and wires were made with a distance of ∼1 cm on the surfaces of the graphene−GO (rGO) hybrid films. Due to the fact that the resistance was bulk limited and the contribution from the contact interface was minimal,[16,17] the total resistance in Figure 3a was mainly governed by the resistance of the hybrid film, in contrast to the case of bottom electrodes contacted in which the film was significantly bended to introduce a local potential barrier. Temperatures were controlled by a hot plate and $I-V$ characterization of the hybrid film was done (by using Keithley 2602) after a certain temperature was achieved, from which the resistance could be calculated. During the test, at the same temperature, three $I-V$ curves were captured and the interval was ∼5 min. It is found that these $I-V$ curves coincided together and the resistance at certain temperature was averaged by the three calculated resistances (in most cases, these three calculated resistances were almost equal), which demonstrated that the resistivity of the hybrid films remains nearly constant with time at the same temperature.

■ ASSOCIATED CONTENT

Supporting Information

Additional experimental data: SEM images, UV−vis spectra, $I-V$ characterizations, XPS spectra, AFM image, XRD profiles, and band diagram. This material is available free of charge via the Internet at http://pubs.acs.org.

■ AUTHOR INFORMATION

Corresponding Author

*E-mail: hongweizhu@tsinghua.edu.cn.

Notes

The authors declare no competing financial interest.

■ ACKNOWLEDGMENTS

This work is supported by the Beijing Natural Science Foundation (2122027), the National Program on Key Basic Research Project (2011CB013000), and Tsinghua University Initiative Scientific Research Program (2012Z02102).

■ REFERENCES

(1) Schafft, H. A.; Suehle, J. S. *Solid-State Electron.* **1992**, *35*, 403−410.
(2) Chi, E. O.; Kim, W. S.; Hur, N. H. *Solid State Commun.* **2001**, *120*, 307−310.
(3) Lin, S.; Wang, B. S.; Lin, J. C.; Huang, Y. N.; Lu, W. J.; Zhao, B. C.; Tong, P.; Song, H. W.; Sun, Y. P. *Appl. Phys. Lett.* **2012**, *101*, 011908.
(4) Phuong, N. M.; Kim, D. J.; Kang, B. D.; Kim, C. S.; Yoon, S. G. *J. Electrochem. Soc.* **2006**, *153*, G27−G29.
(5) Kim, A. T. *Appl. Phys. Lett.* **1997**, *70*, 209−211.
(6) Novoselov, K. S.; Geim, A. K.; Morozov, S. V.; Jiang, D.; Zhang, Y.; Dubonos, S. V.; Grigorieva, I. V.; Firsov, A. A. *Science* **2004**, *306*, 666−669.
(7) Li, X.; Cai, W.; An, J.; Kim, S.; Nah, J.; Yang, D.; Piner, R.; Velamakanni, A.; Jung, I.; Tutuc, E.; Banerjee, S. K.; Colombo, L.; Ruoff, R. S. *Science* **2009**, *324*, 1312−1314.
(8) Kim, K. S.; Zhao, Y.; Jang, H.; Lee, S. Y.; Kim, J. M.; Kim, K. S.; Ahn, J. H.; Kim, P.; Choi, J. Y.; Hong, B. H. *Nature* **2009**, *457*, 706−710.
(9) Chen, S.; Brown, L.; Levendorf, M.; Cai, W.; Ju, S. Y.; Edgeworth, J.; Li, X.; Magnuson, C. W.; Velamakanni, A.; Piner, R. D.; Kang, J.; Park, J.; Ruoff, R. S. *ACS Nano* **2011**, *5*, 1321−1327.
(10) Stankovich, S.; Dikin, D. A.; Piner, R. D.; Kohlhaas, K. A.; Kleinhammes, A.; Jia, Y.; Wu, Y.; Nguyen, S. T.; Ruoff, R. S. *Carbon* **2007**, *45*, 1558−1565.

(11) Eda, G.; Fanchini, G.; Chhowalla, M. *Nat. Nanotechnol.* **2008**, *3*, 270−274.
(12) Ramanathan, T.; Abdala, A. A.; Stankovich, S.; Dikin, D. A.; Herrera-Alonso, M.; Piner, R. D.; Adamson, D. H.; Schniepp, H. C.; Chen, X.; Ruoff, R. S.; Nguyen, S. T.; Aksay, I. A.; Prud'homme, R. K.; Brinson, L. C. *Nat. Nanotechnol.* **2008**, *3*, 327−331.
(13) Manga, K. K.; Zhou, Y.; Yan, Y.; Loh, K. P. *Adv. Funct. Mater.* **2009**, *19*, 3638−3643.
(14) Sun, P.; Ma, R.; Wang, K.; Zhong, M.; Wei, J.; Wu, D.; Sasaki, T.; Zhu, H. *Nanotechnology* **2013**, *24*, 075601.
(15) Jung, I.; Dikin, D. A.; Piner, R. D.; Ruoff, R. S. *Nano Lett.* **2008**, *8*, 4283−4287.
(16) Eda, G.; Mattevi, C.; Yamaguchi, H.; Kim, H.; Chhowalla, M. *J. Phys. Chem. C* **2009**, *113*, 15768−15771.
(17) Kaiser, A. B.; Gomez-Navarro, C.; Sundaram, R. S.; Burghard, M.; Kern, K. *Nano Lett.* **2009**, *9*, 1787−1792.
(18) Sun, P.; Zhu, M.; Wang, K.; Zhong, M.; Wei, J.; Wu, D.; Cheng, Y.; Zhu, H. *Appl. Phys. Lett.* **2012**, *101*, 053107.
(19) Gu, W.; Zhang, W.; Li, X.; Zhu, H.; Wei, J.; Li, Z.; Shu, Q.; Wang, C.; Wang, K.; Shen, W.; Kang, F.; Wu, D. *J. Mater. Chem.* **2009**, *19*, 3367−3369.
(20) Sun, P.; Zhu, M.; Wang, K.; Zhong, M.; Wei, J.; Wu, D.; Xu, Z.; Zhu, H. *ACS Nano* **2013**, *7*, 428−437.
(21) Tapaszto, L.; Nemes-Incze, P.; Dobrik, G.; Yoo, K. J.; Hwang, C.; Biro, L. P. *Appl. Phys. Lett.* **2012**, *100*, 053114.
(22) Yazyev, O. V.; Louie, S. G. *Nat. Mater.* **2010**, *9*, 806−809.
(23) Tsen, A. W.; Brown, L.; Levendorf, M. P.; Ghahari, F.; Huang, P. Y.; Havener, R. W.; Ruiz-Vargas, C. S.; Muller, D. A.; Kim, P.; Park, J. *Science* **2012**, *336*, 1143−1146.
(24) Jauregui, L. A.; Cao, H.; Wu, W.; Yu, Q.; Chen, Y. P. *Solid State Commun.* **2011**, *151*, 1100−1104.
(25) Gomez-Navarro, C.; Weitz, R. T.; Bittner, A. M.; Scolari, M.; Mews, A.; Burghard, M.; Kern, K. *Nano Lett.* **2007**, *7*, 3499−3503.
(26) Vaskol, F. T.; Ryzhii, V. *Phys. Rev. B* **2007**, *76*, 233404.
(27) Shao, Q.; Liu, G.; Teweldebrhan, D.; Balandi, A. A. *Appl. Phys. Lett.* **2008**, *92*, 202108.
(28) Schedin, F.; Geim, A. K.; Morozov, S. V.; Hill, E. W.; Blake, P.; Katsnelson, M. I.; Novoselov, K. S. *Nat. Mater.* **2007**, *6*, 652−655.
(29) Hwang, E. H.; Sarma, S. D. *Phys. Rev. B* **2007**, *76*, 195421.
(30) Wehling, T. O.; Lichtenstein, A. I.; Katsnelson, M. I. *Appl. Phys. Lett.* **2008**, *93*, 202110.
(31) Levesque, P. L.; Sabri, S. S.; Aguirre, C. M.; Guillemette, J.; Siaj, M.; Desjardins, P.; Szkopek, T.; Martel, R. *Nano Lett.* **2011**, *11*, 132−137.
(32) Chakrapani, V.; Angus, J. C.; Anderson, A. B.; Wolter, S. D.; Stoner, B. R.; Sumanasekera, G. U. *Science* **2007**, *318*, 1424−1430.
(33) Jung, I.; Dikin, D.; Park, S.; Cai, W.; Mielke, S. L.; Ruoff, R. S. *J. Phys. Chem. C* **2008**, *112*, 20264−20268.
(34) Chang, H.; Sun, Z.; Yuan, Q.; Ding, F.; Tao, X.; Yan, F.; Zheng, Z. *Adv. Mater.* **2010**, *22*, 4872−4876.